

PACS numbers: 42.55.Px; 42.60.Jf
DOI: 10.1070/QE2008v038n12ABEH013819

Photoinduced and thermal reactions involving hydrogen in high-germania-core optical fibres

A.O. Rybaltovskii, V.V. Koltashev, O.I. Medvedkov, A.A. Rybaltovskii, V.O. Sokolov, S.N. Klyamkin, V.G. Plotnichenko, E.M. Dianov

***Abstract*. We report a Raman scattering study of photoinduced and thermal reactions between H_2 and germanosilicate optical fibres with 22 mol % and 97 mol % GeO_2 in the core (F1 and F2, respectively) after H_2 loading at 150 MPa (1500 atm). The mechanisms of photoreactions are investigated in a wide range of incident laser wavelengths (244, 333, 354, 361 and 514 nm). Thermal reactions are studied at 500 °C. The results indicate that the main mechanism behind the formation of hydrogen-containing defects with Raman bands at 700, 750, 2190, 3600 and 3680 cm^{-1} involves $\equiv Ge-O-Ge\equiv$ or $\equiv Ge-O-Si\equiv$ bond breaking and formation of hydride and hydroxyl species: $=GeH_2$ (700, 750 cm^{-1}), $\equiv Ge-H$ (2190 cm^{-1}), $\equiv GeO-H$ (3600 cm^{-1}) and $\equiv SiO-H$ (3680 cm^{-1}). The key features of the reactions in the F1 and F2 fibres are analysed. In particular, photoinduced reactions give $\equiv Si-OH$ groups only in the F1 fibres, whereas the formation of germanium nanoclusters at a relatively low temperature (~500 °C) or $\equiv GeO-H$ and $\equiv Ge-H$ defects under 514-nm irradiation has only been observed in the F2 fibres.**

Keywords: *germanosilicate fibres, photosensitivity, germanium nanoclusters, photochemical reactions, molecular hydrogen.*

1. Introduction

Single-mode optical fibres with high-GeO_2 (20 mol % to 100 mol %) cores enable the fabrication of efficient visible and near-IR Raman lasers and amplifiers [1]. Such fibres exhibit markedly higher 1300- to 1700-nm optical losses (~10 dB km^{-1}) in comparison with standard telecom fibres (0.2 – 0.3 dB km^{-1}) but offer a larger non-linear response [2] and, as shown recently [3 – 5], higher photosensitivity.

The mechanisms responsible for the photosensitivity of fibres with germanosilicate glass cores and approaches to enhancing it, in particular, molecular hydrogen (H_2) loading, have been studied since the early 1990s [6, 7]. This is mainly associated with the need for efficient fibre Bragg grating inscription techniques and is of particular importance in creating fibre Raman lasers and amplifiers, in which index gratings act as mirrors [8].

The first results on index changes induced in heavily doped germanosilicate fibres by near-UV laser radiation were reported by Dianov et al. [3]. Based on the known mechanisms of photochemical reactions involving H_2 molecules, they made an attempt to explain the observed distinctions between the fluence dependences of index changes in fibres containing 22 mol % and 97 mol % GeO_2. Like in the case of relatively low C_{GeO_2} concentrations [9, 10], Raman scattering studies of photosensitivity in such fibres provide detailed insight into the mechanisms of chemical reactions involving H_2 molecules in the GeO_2 network because they allow one to examine the effects of UV irradiation and high temperature on the intensity of Raman bands related to the glass network.

Note that there remain a number of unanswered questions about the role of germanium-related oxygen-deficient centres (GeODCs), which are believed to be involved in index grating formation [11], and about the contribution that the hydride and hydroxyl species resulting from reactions with H_2 molecules [12, 13] make to index changes.

Here we report a Raman scattering study of photo- and thermochemical reactions involving H_2 molecules in heavily doped germanosilicate fibres with $C_{GeO_2} = 97$ % in the core, loaded with hydrogen at a pressure of 150 MPa. For comparison with previous results, we also investigated fibres with $C_{GeO_2} = 22$ %. This article presents the continuation of our previous research on photo- and thermally induced effects in germanosilicate fibres with lower GeO_2 contents [3, 14 – 17]. Through high-pressure hydrogen loading treatment of the fibres, we hoped to gain further insight into chemical reactions between H_2 molecules and the core of germanosilicate fibres exposed to UV laser radiation or elevated temperatures.

2. Experimental

We studied three types of fibres with germanosilicate glass cores:

A.O. Rybaltovskii D.V. Skobel'tsyn Institute of Nuclear Physics, M.V. Lomonosov Moscow State University, Vorob'evy gory, 119992 Moscow, Russia; e-mail: aor@raven.phys.msu.ru;
V.V. Koltashev, O.I. Medvedkov, A.A. Rybaltovskii, V.O. Sokolov, V.G. Plotnichenko, E.M. Dianov Fiber Optics Research Center, Russian Academy of Sciences, ul. Vavilova 38, 119333 Moscow, Russia; e-mail: kvv@fo.gpi.ru, medoi@fo.gpi.ru, andy@fo.gpi.ru, vvvl@bigfoot.com, victor@fo.gpi.ru, dianov@fo.gpi.ru;
S.N. Klyamkin Department of Chemistry, M.V. Lomonosov Moscow State University, Vorob'evy gory, 119992 Moscow, Russia; e-mail: klyamkin@highp.chem.msu.ru

Received 2 February 2008; revision received 1 April 2008
Kvantovaya Elektronika **38** (12) 1147 – 1154 (2008)
Translated by O.M. Tsarev

(i) single-mode fibre with a core diameter $2a = 2$ μm and $C_{GeO_2} = 22\,\%$ in the core (F1),

(ii) single-mode fibre with $2a = 1.8$ μm and $C_{GeO_2} = 97\,\%$ (F2a), and

(iii) multimode fibre with $2a = 8$ μm and $C_{GeO_2} = 97\,\%$ (F2b).

The fibres were drawn from MCVD preforms at 1900 °C. Fibre samples were hydrogenated in a high-pressure chamber at 100 °C and 150 MPa (1500 atm) for 24 h. The same hydrogenation procedure was used previously in studies of the spectroscopic properties and diffusion of H_2 molecules in germanosilicate fibres with a relatively low GeO_2 content (5 % to 24 %) of the core [14, 15]. Dianov et al. [3] investigated the photosensitivity of F1 and F2a samples hydrogenated at 12 MPa.

The fibres were irradiated using three Spectra Physics argon lasers: frequency-doubled ($\lambda = 244$ nm) 2040E (hereafter, laser A); BeamLok 2085 operating at 333, 351 and 364 nm (laser B); and Stabilite 2017 (laser C), which was employed as a 514-nm excitation source.

The radiation from laser B was directed to one of the fibre-end faces or to a lateral surface from which the polymer coating had been removed. In the case of laser A, the fibres were only irradiated through the lateral surface because the 244-nm absorption in the fibre core considerably exceeded the absorption in the range 333 – 364 nm [2, 18]. Irradiation with laser C was performed through the fibre faces.

The exposed length of the lateral surface was ~10 cm. The main irradiation parameters are listed in Table 1.

Table 1.

Laser	Wavelength/nm	Irradiation direction	Power density/W cm^{-2}	Fluence/kJ cm^{-2}
A	244	through the lateral surface	$\sim 10^4$	1
B	333, 351, 364	through the fibre face	$\sim 5 \times 10^4$	$\sim 10^2$
		through the lateral surface	1.5×10^2	1
C	514.5	through the fibre face	$(1 - 4) \times 10^5$	not determined

The hydrogen-loaded fibres were annealed using a heater controlled by a Miniterm-300 precision temperature controller (OAO MZTA). The furnace was designed so as to ensure a uniform temperature from 50 to 700 °C in the heating zone, with a stability within 2 °C. The inner diameter of the heater was ~2 mm. The system enabled heating rates up to 150 °C min^{-1}, which is an order of magnitude above those in previous annealing experiments [19]. The high heating rate was expected to ensure markedly higher molecular hydrogen concentrations in the thermochemical reactions in the fibre core than those reached previously, because at the H_2 concentration corresponding to a hydrogenation pressure of 150 MPa the rate of H_2 outdiffusion from the core is an order of magnitude higher [15].

In Raman measurements, excitation was provided by laser C through an Olympus BH2-UMA microscope. Stokes-shifted Raman spectra were measured in a backscattering geometry from 10 to 4000 cm^{-1} with a resolution of ~1 cm^{-1}, using a Jobin Yvon T64000 triple spectrometer equipped with a liquid-nitrogen-cooled CCD array. All the spectra were normalised to the intensity of the fundamental Raman band of germanosilicate glass, centred around 430 cm^{-1} [14].

3. Experimental results and discussion

3.1 3.1 Photoinduced reactions

Figure 1 shows the Raman spectra of the hydrogen-loaded fibres after the shortest wavelength irradiation (laser A). At frequencies above 1000 cm^{-1}, the spectra contain photoinduced Raman bands centred at 2190 and 3600 cm^{-1}. The 2190-cm^{-1} band is similar in shape and position to the 2185-cm^{-1} Raman band reported for germanosilicate glasses containing about 10 % C_{GeO_2} [9], which was assigned to the $\equiv$Ge – H hydride species. The 3600-cm^{-1} band is due to the hydrogens of hydroxyls bonded to germanium ($\equiv$GeO – H) [20]. As shown earlier [21], this band typically has a complex shape and consists of several components corresponding to different conditions of $\equiv$Ge – O defect formation in the glass network [20, 21]. Note that the bands at 2190 and 3600 cm^{-1} in the spectra of the F1 samples are more complex in shape than those of the F2 fibres.

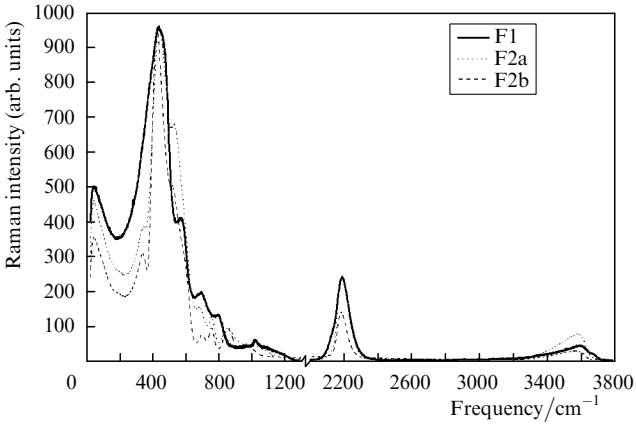

Figure 1. Raman spectra of the hydrogen-loaded fibres after irradiation with laser A.

In addition, at frequencies below 1000 cm^{-1} we observe a marked increase in the intensity of the feature at 540 cm^{-1}, which is commonly assigned to small rings of SiO_4 and GeO_4 tetrahedra in the glass network [10, 22]. It should be emphasised that the increase in the 540-cm^{-1} Raman intensity in the F1 samples is at least one order of magnitude above that in fibres with $C_{GeO_2} = 18\,\%$ irradiated to the same fluence without hydrogenation [10, 22].

After hydrogen loading followed by UV irradiation at 5.08 or 3.72 eV, the Raman spectra of the F2 samples show well-defined features at about 700 and 750 cm^{-1}, respectively (Figs 1, 2). To our knowledge, this is the first observation of these features in the Raman spectra of GeO_2-doped optical fibres, which thus have not been described in the literature. At the same time, similar IR bands, centred at 630 and 830 cm^{-1}, were reported for a-Ge : H films [23] and were tentatively assigned to the $=GeH_2$ centre. Given that in our experiments the 700- and 750-cm^{-1} features were only observed in the Raman

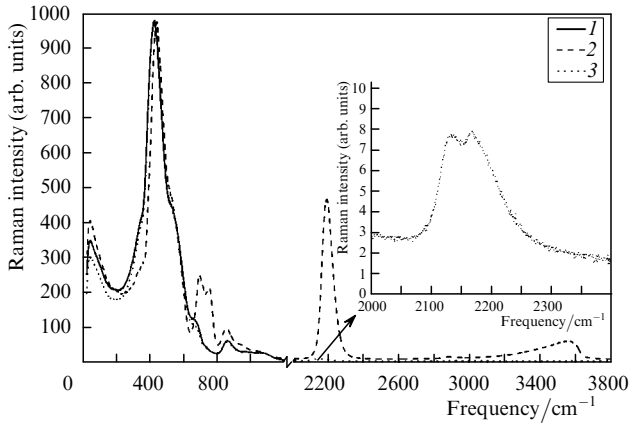

Figure 2. Raman spectra of a hydrogen-loaded F2a sample before irradiation (*1*) and after irradiation with laser B through the fibre face (*2*) and lateral surface (*3*).

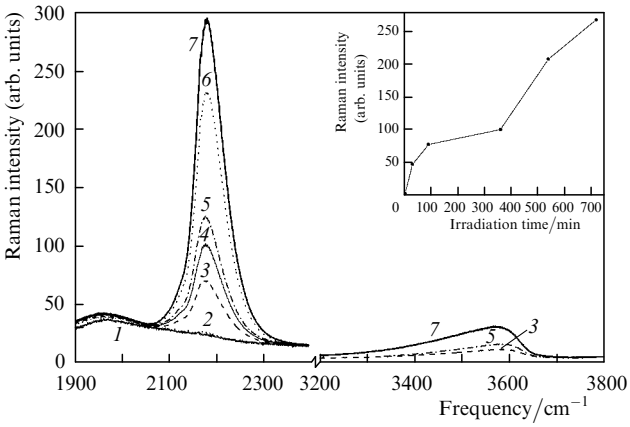

Figure 3. Raman spectra of the F2a sample (*1*) before irradiation and after (*2*) 2 min, (*3*) 30 min, (*4*) 1.5 h and (*5*) 6 h of irradiation with laser C; (*6*, *7*) after further irradiation for 3 and 6 h, respectively, following a 15-h break. Inset: intensity of the 2190-cm^{-1} band as a function of irradiation time.

spectra of the F2 samples (GeO_2 content close to 100 %), similar assumptions can be made as to the nature of the defects involved. It is quite possible that, as in the case of a-Ge : H films, the 700- and 750-cm^{-1} features arise from the $=GeH_2$ centres produced by UV radiation in the core of the hydrogen-loaded F2 fibres.

In our opinion, the effect of irradiation at 3.72, 3.53 and 3.41 eV (laser B) on the Raman spectra of the F2a samples is of special interest for gaining insight into the associated photoinduced reactions. The relevant results are presented in Fig. 2. One can see that, at frequencies above 1000 cm^{-1}, the Raman bands obtained under irradiation through the fibre face are very similar in shape to those of the F2a sample irradiated at a higher photon energy (5.08 eV). The spectra show prominent bands centred at 2190 and 3600 cm^{-1}. At the same time, after irradiation through the lateral surface to a fluence of 1 kJ cm^{-2} these bands are much weaker and more complex in shape. The 2190-cm^{-1} band consists of two distinct components, and the intensity of the 3600-cm^{-1} band is close to the noise level. The higher intensity of the Raman bands induced by irradiation through the fibre face in comparison with irradiation through the lateral surface is due to the higher irradiation fluence (Table 1). According to earlier results [2, 18], the absorption in GeO_2-rich germanosilicate glass between 330 and 360 nm is 0.3–0.5 dB mm^{-1}, which is an order of magnitude below that near 240 nm. From this value and the irradiation time ($\sim$5 min), the average fluence delivered to a $\sim$10-cm-long fibre can be estimated at 10^2 J cm^{-2}. This estimate accounts for the higher observed intensity of the Raman bands induced by irradiation through the fibre face in comparison with irradiation through the lateral surface. Moreover, the radiation-induced Raman bands of hydride and hydroxyl species are comparable in intensity to those obtained under 5.08-eV irradiation to a lower fluence of 1 kJ cm^{-2} (Figs 1, 2).

Irradiation of F2a and F2b samples with laser C (514.5 nm; photon energy, 2.41 eV) also gave rise to Raman bands of hydride and hydroxyl species. In the spectra of the F1 samples, no such bands were detected. Figure 3 shows the Raman spectra of the F2a fibre in the 2190-cm^{-1} region for various irradiation times. The intensity of the 2190-cm^{-1} band is seen to markedly increase with irradiation time. Nevertheless, in spite of the high incident power density (4×10^5 W cm^{-2}) the intensity of this band remains well below that under higher energy irradiation. The most likely reason for this is that the 514-nm absorption in germanosilicate glass is much weaker (by several orders of magnitude) than the absorption at wavelengths below 360 nm [18].

It is of interest to note the behaviour of the 2190-cm^{-1} Raman band during irradiation with laser C: its intensity rose at a gradually decreasing rate during irradiation, but after a 15-h break a steep rise was again observed. As seen in the inset in Fig. 3, the steady rise in the intensity of this band is followed by saturation at irradiation times longer than 100 min, which gives way to a rise in intensity during further irradiation after the 15-h break (during which the fibre was kept under normal conditions).

The rise in intensity during irradiation after the break may be due to the relaxation of the glass network, which is necessary for photochemical reactions involving H_2 molecules: the H_2 concentration in the irradiated region of the core increases as a result of hydrogen indiffusion from the reflective cladding. The diffusion is driven by the reduction in H_2 concentration in the core as a result of photochemical reactions between H_2 and components of the glass network [24].

Another possible reason is the rise in the power of the exciting radiation passing through the fibre due to its weaker scattering because most of the molecular hydrogen left the core during the 15-h break [15]. This assumption is supported by the following experimental observation: during the second irradiation cycle, whose duration was about the same as that of the first cycle (before the break), the intensity of the 2190-cm^{-1} Raman band increased twofold. This effect is much more sensitive to the H_2 concentration than is the increase in the refractive index [24], which is also proportional to the concentration of hydrogen diffusing from the cladding to the core of the irradiated fibre.

Consider now the formation of photoinduced hydrogen-containing species in the fibres using the present experimental data and earlier results on photochemical reactions involving H_2 in the germanosilicate glass network. As shown previously [9, 12, 25], UV laser irradiation of H_2-loaded germanosilicate glass leads to the formation of hydrogen-

containing defects, such as $\equiv Ge-H$, $\equiv GeO-H$, and $\equiv SiO-H$, through the following photochemical reactions:

$$\equiv Ge-O-Ge\equiv +H_2 \xrightarrow{h\nu} \equiv Ge-H+H-OGe\equiv, \quad (1)$$

$$\equiv Ge-O-Si\equiv +H_2 \xrightarrow{h\nu} \equiv Ge-H+H-OSi\equiv. \quad (2)$$

Moreover, UV irradiation of germanosilicate glass with a high concentration of GeODC-type defects may lead to the capture of H_2 molecules by such defects [9, 13, 25], resulting in the formation of other hydrogen-containing centres, $=GeH_2$, with a Raman band near 2140 cm^{-1}:

$$=Ge: +H_2 \xrightarrow{h\nu} =GeH_2. \quad (3)$$

The presence of GeODCs in the glass network of the cores of the fibres under consideration is supported by the strong absorption band at 242 nm in the UV transmission spectra of the preforms from which the fibres were drawn [2, 18]. Judging from the intensity of the 242-nm band, the GeODC concentration in the F2 samples is lower than that in F1 [2]. On the whole, the GeODC concentration in the fibre samples studied is two to three orders of magnitude below the total concentration of $\equiv Ge-O-Ge\equiv$ or $\equiv Ge-O-Si\equiv$ structural units, which are potentially capable of participating in reactions (1) and (2). The core of the single-mode F2 fibres contains a larger amount of strained bonds in comparison with the multimode fibres. Under identical UV irradiation conditions, this leads to a more significant photoinduced increase in the intensity of the Raman bands at 2190 and 3600 cm^{-1}. In other words, the photoinduced reaction (1) is more efficient in the single-mode fibre than in the multimode one.

The effects of reactions (2) and (3) are most pronounced in the F1 samples. One can see in Figs 1 and 4a that, as mentioned above, the Raman bands at 2190 and 3600 cm^{-1} have a rather complex shape. In particular, the 2190-cm^{-1} band has a significant contribution from the $=GeH_2$ centre, with a maximum at 2140 cm^{-1}. The Raman scattering around 3600 cm^{-1} is contributed by a component at 3670 cm^{-1}, due to $\equiv SiO-H$ silanol centres [21]. The 2190-cm^{-1} band of the F2a samples has a complex shape after irradiation at 3.72, 3.53 and 3.41 eV through the lateral surface (Fig. 2), and even after 2.41-eV irradiation if the exposure time is within 90 min (Fig. 3). It seems likely that photochemical reaction (3) takes place in the F2 fibres as well. It is therefore reasonable to assume that the lower frequency component at $\sim$2130 cm^{-1} is due to the radiation-induced $=GeH_2$ centres in the glass which consists almost entirely of GeO_2. The lower frequency of this component compared to the 2140-cm^{-1} band is probably associated with the markedly higher GeO_2 concentration in the core of the F2a sample. With increasing irradiation fluence, the contribution of the $\equiv Ge-H$ centre to the 2190-cm^{-1} Raman band becomes predominant, while the lower frequency component almost completely disappears. Under 2.41-eV irradiation, photochemical reactions may be initiated by both one- and two-photon absorption in $\equiv Ge-O-Ge\equiv$ bridges. To identify the mechanism of the photochemical reactions in question, the intensity of the 2190-cm^{-1} band must be measured as a function of laser radiation power.

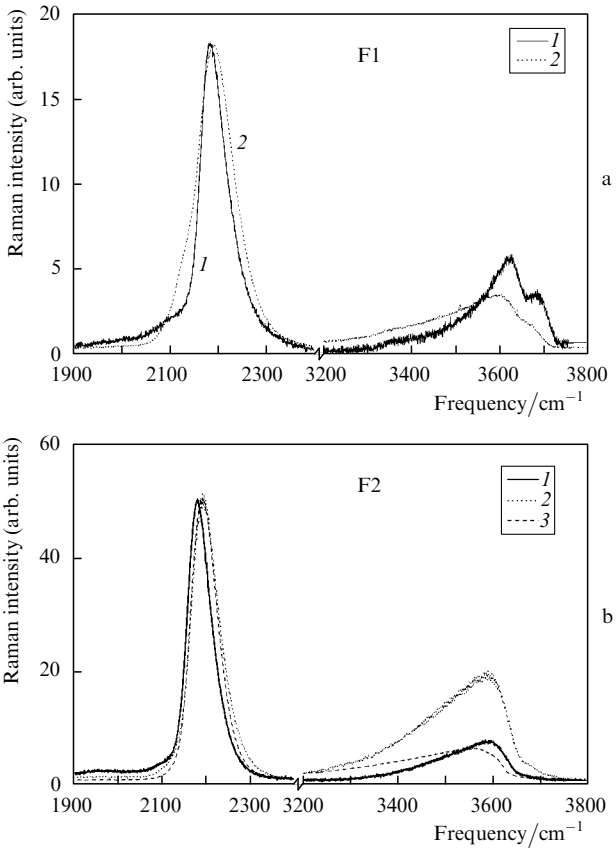

Figure 4. Raman spectra of (a) F1 and (b) F2 samples after (*1*) annealing at 500 °C and (*2*, *3*) irradiation; (*2*) laser A, (*3*) laser B.

The relative intensities of the Raman bands at 2190 and 3600 cm^{-1} in the irradiated F2a samples (Figs 1–3) point to the following tendency: with decreasing incident photon energy, the intensity ratio of these bands increases. It is therefore likely that, in addition to reaction (1), which gives identical amounts of hydride and hydroxyl centres, at least one mechanism is also responsible for the formation of $\equiv Ge-H$ centres in the F2a samples. Its contribution is particularly significant under low-energy irradiation. It should be emphasised that it is not $\equiv Ge-O-Ge\equiv$ bridge breaking which underlies this mechanism. One possibility is that the core of the F2 samples contains considerably more microregions enriched in germanium (with a nonstoichiometric composition, GeO_{2-x}) or even pure Ge clusters several nanometers or less in size [14] than does the core of the F1 samples. The boundaries of such regions contain significant amounts of strained bonds, which effectively respond to laser irradiation and react with hydrogen to form $\equiv Ge-H$ centres, without compensation by $\equiv GeO-H$ centres. It is quite likely that the presence of many microregions enriched in Ge nanoclusters in the core of the F2 samples will be favourable for non-linear conversion of laser radiation in the fibre.

3.2 Thermochemical reactions

Consider thermochemical reactions involving H_2 and how they show up in the Raman spectra of the fibres studied. Figures 4 and 5 present the Raman spectra of F1 and F2a samples after hydrogenation followed by thermal annealing at 500 °C. As in the case of irradiation, the dominant process in both fibres is reaction (1), which leads to the

formation of $\equiv Ge-H$ и $\equiv GeO-H$ centres, with the corresponding Raman bands at 2190 and 3600 cm^{-1}. The spectrum of the F1 sample, like that after irradiation, shows a feature at 3670 cm^{-1}, which arises from $\equiv SiO-H$ centres (Fig. 4a).

Nevertheless, there are certain distinctions between the mechanisms underlying the formation of photo- and thermochemical reaction products in hydrogen-loaded fibres with high-GeO_2 cores.

One distinctive feature of the thermochemical reactions in germanosilicate fibres is that, in the Raman spectra of the annealed fibres, the 2140-cm^{-1} band, related to the $\equiv Ge-H_2$ centre, is missing, in contrast to the spectrum of the irradiated F1 sample (Fig. 1). This feature was pointed out earlier by Greene et al. [9], who analysed the Raman spectra of fibres with 10 % GeO_2 in the core after hydrogen loading at ~ 10 MPa, UV irradiation and thermal annealing. Moreover, according to Awazu et al. [26] thermochemical reactions between H_2 and germanosilicate glass are quite likely to produce GeODCs:

$$\equiv Ge-O-Ge\equiv +H_2 \xrightarrow{t^0} =Ge:+2(H-O-Ge\equiv). \quad (4)$$

It may be that reaction (4) is responsible for the increase in the intensity of the Raman band at 3600 cm^{-1} relative to that at 2190 cm^{-1}, the effect being more pronounced during heat treatment than during 5.04 eV irradiation. Note that Atkins and Espindola [27] interpreted the annealing-induced rise in the intensity of the GeODC-related absorption band at 242 nm in hydrogen-loaded germanosilicate fibres as evidence for reaction (4).

Another noteworthy feature of the thermochemical reactions involving H_2 molecules is that the low-frequency wing of the 3600-cm^{-1} band in the spectra of the annealed F1 and F2 samples differs in shape from that in the spectra of the irradiated samples (Fig. 4). This is probably due to the reduction in the contribution of the 3530-cm^{-1} component, which was attributed in an earlier study [20] to $\equiv Ge-OH$ centres linked by weak hydrogen bonds to $\equiv Ge-O-Ge\equiv$ bridges. It is quite possible that such centres are unstable at the annealing temperature we used (500 °C) and, hence, have an insignificant effect on the formation of hydroxyl centres in the glass network.

Unlike irradiation, thermal annealing of the fibres slightly shifts the 2190-cm^{-1} Raman band to lower frequencies (by no more than 10 cm^{-1}) and reduces its full width at half maximum by about 20 % (Fig. 4). This is due to the higher degree of relaxation in the environment of hydride centres directly during their thermally induced formation.

The Raman spectrum of the annealed F2a sample shows features at 700 and 750 cm^{-1} (Fig. 5), which were assumed above to arise from the $=GeH_2$ centre because similar features were observed in the spectra of the irradiated samples.

Yet another thermally induced effect in the hydrogen-loaded fibres is worth noting. After annealing at 500 °C, the Raman spectra of some of the F2a samples showed a band at 297 cm^{-1} (Fig. 5). This band is similar to that observed earlier at lower GeO_2 contents (20 % – 30 %) and is due to the Ge nanoclusters formed during heating of the hydrogen-loaded fibre by a gas burner at temperatures above 1000 °C. In this study, no Ge nanoclusters were detected in the F1

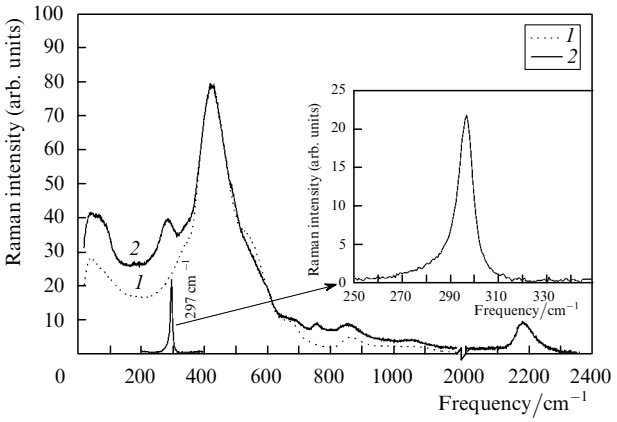

Figure 5. Raman spectra of an F2a sample (*1*) before and (*2*) after annealing at 500 °C for 30 min. The 297-cm^{-1} band observed after the anneal is due to germanium nanoclusters.

samples annealed at 500 °C, which were similar in properties to the fibres investigated previously [14].

The irreproducible formation of Ge nanoclusters in the F2 samples, with marked variations from section to section, is most likely associated with longitudinal variations in core parameters, such as the stress at the core – cladding interface or the concentration of nanocluster precursors (no greater than 2 nm in size), which cannot be detected by Raman spectroscopy. The factors that influence the formation of Ge nanoclusters in hydrogen-loaded fibres were analysed in previous reports [14, 17].

3.3 Concentration of hydride groups in high-GeO_2 fibre

The concentration of photoinduced $\equiv Ge-H$ groups in the core of the F2a fibre can be estimated from Raman results using quantum-chemical modelling.

It should be emphasised that, when comparing Raman intensities to one another and to calculation results, one must use the 'reduced' Raman spectrum [28, 29]:

$$I_r(\omega_{las},\Omega) \propto I_m(\omega_{las},\Omega)\frac{\Omega}{n(\Omega)+1}\frac{1}{(\omega_{las}-\Omega)^4}, \quad (5)$$

where I_r is the reduced Raman intensity; I_m is the measured Raman intensity; ω_{las} is the frequency of the incident (laser) light; Ω is the Stokes shift; and $n(\Omega) = [\exp(\hbar\Omega/kT) - 1]^{-1}$ is the Bose distribution function for phonons at the Stokes frequency.

Figure 6 shows the reduced Raman spectrum of irradiated hydrogen-loaded germanosilicate glass. The band at 2190 cm^{-1} arises from H – Ge stretches in the $\equiv Ge-H$ group, and that around 430 cm^{-1} is due to the A_1 bending mode of the $\equiv Ge-O-Ge\equiv$ bridge. Both bands were fitted with a Voigt function using chi-square minimisation (Fig. 6, thin lines). The best-fit frequencies thus determined are 2194 ± 2 and 443 ± 1 cm^{-1}. The intensity ratio of these bands, evaluated as the ratio of the areas under the best-fit profiles, is about 3 : 1.

In our simulations, the germanate component of the glass network and the $\equiv Ge-H$ group were represented by the $(GeO)_3\equiv Ge-O-Ge\equiv(GeO)_3$ and $H-Ge\equiv(GeO)_3$ clusters, respectively. The dangling bonds of the Ge atoms were saturated with hydrogen atoms. All computations were performed with the GAMESS package [30] within the local-density-functional approach, using the BLYP functional,

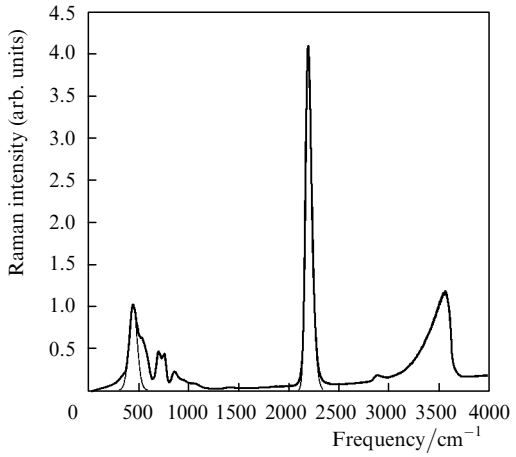

Figure 6. Model (reduced) Raman spectrum of irradiated hydrogen-loaded germanosilicate glass.

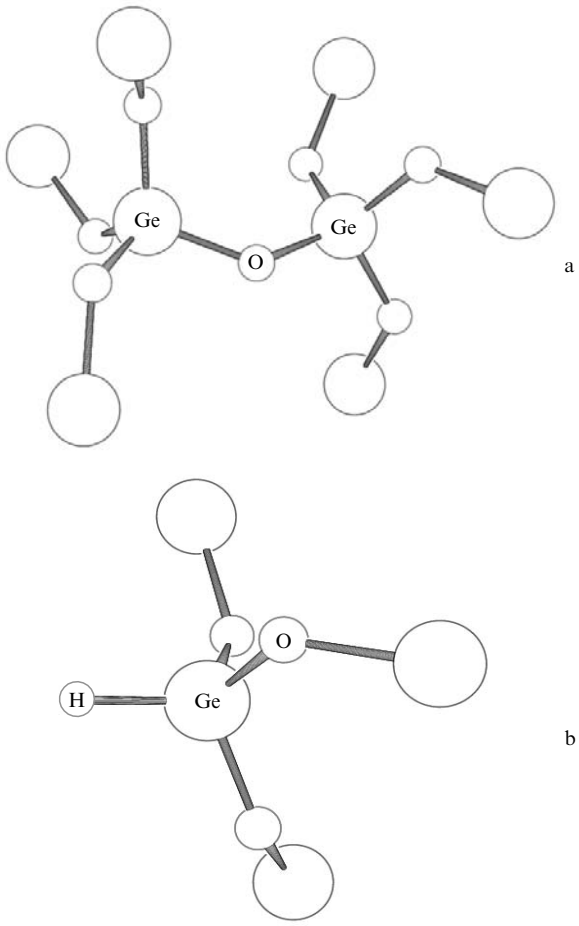

Figure 7. Simulated configurations of the (a) $(GeO)_3 \equiv Ge-O-Ge \equiv (GeO)_3$ bridge and (b) $H-Ge \equiv (GeO)_3$ group in the germanosilicate glass network.

which is known to ensure the best agreement between calculated and experimentally determined geometric parameters and vibrational frequencies. We used the basis sets and effective core potentials proposed in [31, 32], with a d polarisation function added to the basis sets of the oxygen and germanium atoms (orbital exponent $\zeta = 0.8000$ and 0.2460 Bohr^{-1}, respectively). This basis ensures good description of the properties of systems similar to that under investigation [33, 34]. For the hydrogen atoms that saturated dangling bonds, the standard 3-21G basis set was used.

The simulations included complete optimisation of the geometry of both clusters. The simulated configurations of the $\equiv Ge-O-Ge \equiv$ bridge and $HGeO_3$ group are shown in Fig. 7. The intensity ratio of the Raman bands at 2190 and 430 cm^{-1} was determined to be about 122, and the respective depolarisation ratios are 0.18 and 0.66.

From the observed and calculated Raman intensities, the ratio of the concentration of $\equiv Ge-O-Ge \equiv$ bridges to that of $\equiv Ge-H$ hydride groups in the heavily doped germanosilicate glass was estimated at 39 : 4. Given that the density of the germanosilicate glass is 5.7 g cm^{-3}, we find that the concentration of hydride groups is 6×10^{21} cm^{-3}.

This estimate, as well as some of our conclusions related to the relationship between the concentrations of hydride and hydroxyl species in different fibre samples, is based on the relative intensities of the Raman bands near 430, 2190, and 3600 cm^{-1}. These bands are known to be Stokes components of the 525-, 580-, and 630-nm laser radiation scattered in the fibre core. Therefore, variations in the induced absorption coefficient of the core in the wavelength range 525–630 nm may distort measured Raman intensities. Consequently, in calculations of the relative intensities of the bands at 430, 2190, and 3600 cm^{-1}, a correction for the induced absorption coefficient must be introduced.

The UV-induced absorption above 400 nm in germanosilicate fibres was investigated by Anoikin et al. [35]. This absorption is due to the contribution from the long-wavelength edge of the photoinduced UV absorption bands related to Ge E′ centres. In the visible range, the curve related to the UV absorption is well represented by an exponential, with parameters dependent on the type of fibre and irradiation conditions. In view of this, the absorption coefficient of F1 and F2a samples hydrogenated at 150 MPa and then irradiated with laser A to a fluence of 1 kJ cm^{-2} was measured in the range 400–700 nm.

The results are presented in Table 2, which lists the attenuation coefficients k for 525-, 580- and 630-nm scattered laser radiation (normalised to k at 630 nm). It follows from Table 2 that the correction coefficient k has no significant effect on the intensity ratio of the Raman bands at 3600 and 2190 cm^{-1}. Therefore, the conclusions related to this ratio remain valid. At the same time, k should be taken into account in evaluating the concentration of hydride groups in the F2a fibre from the intensity ratio of the bands at 2190 and 430 cm^{-1}.

Table 2.

Scattered laser radiation wavelength/nm	Raman peak position/cm^{-1}	Attenuation coefficient	
		Sample F1	Sample F2a
630	3600	1	1
580	2190	1.2	1.5
525	430	2	3

Taking into account the effect of induced absorption on the intensity ratio of the Raman bands at 2190 and 430 cm^{-1}, we find that the concentration of radiation-induced $HGeO_3$ groups is 3×10^{21} cm^{-3}.

4. Conclusions

We performed the first Raman scattering study of photo- and thermochemical reactions between molecular hydrogen and high-GeO_2 (up to 97 mol %) core optical fibres loaded with H_2 at 150 MPa (1500 atm).

UV irradiation at a photon energy of 5.08 eV was found to markedly increase the intensity on the high-frequency side of the fundamental Raman band, with a maximum at 540 cm^{-1}, which is commonly assigned to small (three- and four-membered) rings of GeO_4 tetrahedra [10]. After H_2 loading, the increase in the intensity of this feature in germanosilicate glasses is larger by more than an order of magnitude.

After H_2 loading followed by UV irradiation or heat treatment, the Raman spectrum of the fibre with 97 % GeO_2 in the core showed two new Raman features at 700 and 750 cm^{-1}, which were assumed to arise from the $=GeH_2$ centre.

The main reaction initiated by photoexcitation or heat treatment in the 97 % GeO_2 core of the fibres is bond breaking in the $\equiv Ge-O-Ge\equiv$ bridge, followed by stabilisation of the dangling bonds with hydrogen atoms. As a result, the Raman spectra show strong bands at 2190 and 3600 cm^{-1}, due to the formation of $\equiv Ge-H$ and $\equiv GeO-H$ centres in the glass network. Using the reduced Raman spectrum derived from experimental data and quantum-chemical simulation of clusters containing a $\equiv Ge-O-Ge\equiv$ bridge and $\equiv Ge-H$ groups, we estimated the ratio of their concentrations in irradiated hydrogen-loaded fibres. The $\equiv Ge-H$ concentration inferred from these estimates (3×10^{21} cm^{-3}) points to high efficiency of photochemical reactions between hydrogen and the core of such fibres.

In all the fibres studied, photoexcitation initiates reactions between H_2 and GeODCs, leading to the formation of $=GeH_2$ centres. These are responsible for the Raman band near 2140 cm^{-1}, whose contribution to the 2190-cm^{-1} band increases in going from the fibres with $C_{GeO_2}=22\,\%$ to those with $C_{GeO_2}=97\,\%$.

After hydrogenation and thermal annealing, the spectra of the fibres studied do not show the 3530-cm^{-1} component of the hydroxyl band, which corresponds to a $\equiv GeOH$ centre hydrogen-bonded to the oxygen of an $\equiv Ge-O-Ge\equiv$ bridge and is always present in the spectra of germanosilicate fibres after hydrogenation and UV irradiation.

Both heat treatment and photoexcitation give rise to a feature at 3670 cm^{-1} in the Raman spectra of the fibres with $C_{GeO_2}=22\,\%$, in contrast to those with $C_{GeO_2}=97\,\%$. This feature is due to $\equiv Si-OH$ silanol centres in the glass network. The likely reason for the high efficiency of $\equiv Si-OH$ formation in the 22 % GeO_2 fibre core is that the glass network contains a large amount of strained $\equiv Ge-O-Si\equiv$ bridges, capable of participating in thermo- and photochemical reactions.

In the fibres with $C_{GeO_2}=97\,\%$, we have identified a new mechanism of $\equiv Ge-H$ formation, which presumably involves excitation of strained bonds in microregions that either have an increased germanium to oxygen ratio or are very small Ge nanoclusters. This mechanism is operative under irradiation at 3.72 and 2.41 eV but not at 5.08 eV. The first experimental evidence is found for the formation of $\equiv Ge-H$ and $\equiv GeOH$ centres under laser irradiation at a wavelength of 514.5 nm, corresponding to a relatively low photon energy (2.41 eV).

In the hydrogen-loaded heavily doped (97 % GeO_2) germanosilicate fibres, Ge clusters 7–8 nm in size were found to form at a relatively low annealing temperature ($\sim500\,^{\circ}C$), in contrast to the fibres with a GeO_2 content of 22 % in the core.

Acknowledgements. The authors thank A.A. Frolov for his assistance in the experimental work and V.M. Mashinsky for helpful comments and discussions. This work was supported in part by the Russian Foundation for Basic Research (Grant No. 01-02-16848) and the RF President's Grants Council for Support to Leading Scientific Schools (Grant No. NSh-2813.2006.2).

References

1. Dianov E.M., Bufetov I.A., Mashinsky V.M., Neustruev V.B., Medvedkov O.I., Shubin A.V., Mel'kumov M.A., Guryanov A.N., Khopin V.F., Yashkov M.V. *Kvantovaya Elektron.*, **34**, 695 (2004) [*Quantum. Electron.*, **34**, 695 (2004)].
2. Dianov E.M., Mashinsky V.M. *J. Lightwave Technol.*, **23** (11), 3500 (2005).
3. Dianov E.M., Rybaltovskii A.A., Semenov S.L., Guryanov A.N., Khopin V.F. *Kvantovaya Elektron.*, **36**, 145 (2006) [*Quantum. Electron.*, **36**, 145 (2006)].
4. Mashinsky V.M., Neustruev V.B., Dvoyrin V.V., Vasiliev S.A., Medvedkov O.I., Bufetov I.A., Shubin A.V., Dianov E.M., Guryanov A.N., Khopin V.F., Salgansky M.Yu. *Opt. Lett.*, **29** (22), 2596 (2004).
5. Mashinsky V.M., Medvedkov O.I., Neustruev V.B., Dvoyrin V.V., Vasiliev S.A., Dianov E.M., Khopin V.F., Guryanov A.N. *Proc. Europian Conf. Optical Communications (ECOC'2003)* (Rimini, Italy, 2003) Tu 1.7.2.
6. Lemaire P.J., Atkins R.M., Mizrahi V., Reed W.A. *Electron. Lett.*, **29** (13), 1191 (1993).
7. Atkins R.M., Lemaire P.J., Erdogan T., Mizrahi V. *Electron. Lett.*, **29** (14), 1234 (1993).
8. Erdogan T. *J. Ligthwave Technol.*, **15** (8), 1277 (1997).
9. Green B.I., Krol D.M., Kosinski S.G., Lemaire P.J., Saeta P.N. *J. Non-Crystal. Sol.*, **168**, 195 (1994).
10. Dianov E.M., Plotnichenko V.G., Koltashev V.V., Pyrkov Yu.N., Ky N.H., Limberger H.G., Salathe R.P. *Opt. Lett.*, **22** (23), 1754 (1997).
11. Dianov E.M., Sokolov V.O., Sulimov V.B. *Kvantovaya Elektron.*, **24**, 617 (1997) [*Quantum. Electron.*, **27**, 600 (1997)].
12. Dalle C., Cordier P., Depecker C., Niay P., Bernage P., Douay M. *J. Non-Crystalline Sol.*, **260**, 83 (1999).
13. Grubsky V., Starodubov D.S., Feinberg J. *Opt. Lett.*, **24** (11), 729 (1999).
14. Plotnichenko V.G., Rybaltovskii A.O., Sokolov V.O., Koltashev V.V., Malosiev A.R., Popov V.K., Dianov E.M. *J. Non-Crystal. Sol.*, **281**, 25 (1999).
15. Plotnichenko V.G., Vasiliev S.A., Rybaltovskii A.O., Koltashev V.V., Sokolov V.O., Klyamkin S.N., Medvedkov O.I., Rybaltovski A.A., Malosiev A.R., Dianov E.M. *J. Non-Crystal. Sol.*, **351**, 3677 (2005).
16. Vasiliev S.A., Medvedkov O.I., Plotnichenko V.G., Dianov E.M., Rybaltovskii A.O. *Opt. Lett.*, **31** (1), 11 (2006).
17. Malosiev A.R., Plotnichenko V.G., Rybaltovskii A.O., Sokolov V.O., Koltashev V.V. *Neorg. Mater.*, **39**, 374 (2003).
18. Mashinsky V.M., Dianov E.M., Neustruev V.B., Lavrishchev S.V., Guryanov A.N., Khopin V.F., Vechkanov N.N. *Proc. SPIE Int. Soc. Opt. Eng.*, **2290**, 105 (1994).
19. Kusvanto H., Goutland F., Yahya A., Boukenter A., Querdane Y. *J. Non-Crystal. Sol.*, **280**, 277 (2001).
20. Plotnichenko V.G., Sokolov V.O., Dianov E.M. *J. Non-Crystal. Sol.*, **278**, 85 (2000).
21. Plotnichenko V.G., Sokolov V.O., Mashinsky V.M., Sidorov V.A., Guryanov A.N., Khopin V.F., Dianov E.M. *J. Non-Crystal. Sol.*, **296**, 88 (2001).

22. Vasiliev S.A., Dianov E.M., Koltashev V.V., Marchenko V.M., Mashinsky V.M., Medvedkov O.I., Plotnichenko V.G., Pyrkov Yu.N., Sazhin O.D., Frolov A.A., *Kvantovaya Elektron*., **25**, 341 (1998) [*Quantum. Electron*., **25**, 330 (1998)].
23. Nadzhafov B.A., Isakov G.I. *J. Appl. Spectroscopy*, **72** (3), 396 (2005).
24. Jang J.N., Kim H.G., Shin S.G., Kim M.S., Lee S.B., Kwack K.H. *J. Non-Crystal. Sol*., **259**, 156 (1999).
25. Lancry M., Poumellec B., Niay P., Douay M., Cordier P., Depecker C. *J. Non-Crystal. Sol*., **351**, 3773 (2005).
26. Awazu K., Kawazoe H., Yamane M. *J. Appl. Phys*., **68** (6), 2713 (1990).
27. Atkins R.M., Espindola R.P. *Appl. Phys. Lett*., **70**, 1068 (1997).
28. Galeener F.L., Sen P.N. *Phys. Rev. B*, **17** (4), 1928 (1978).
29. Plotnichenko V.G., Sokolov V.O., Dianov E.M., Koltashev V.V., Grishin I.A., Churbanov M.F. *Opt. Lett*., **30** (10), 1156 (2005).
30. Schmidt M.W., Baldridge K.K., Boatz J.A., Elbert S.T., Gordon M.S., Jensen J.J., Koseki S., Matsunaga N., Nguyen K.A., Windus T.L., Dupuis M., Montgomery J.A. *J. Comput. Chem*., **14**, 1347 (1993).
31. Stevens W.J., Balsch H., Krauss M. *J. Chem. Phys*., **81** (12), 6026 (1984).
32. Gundary T.R., Stevens W.J. *J. Chem. Phys*., **98** (7), 5555 (1993).
33. Amado A.M., Ribeiro-Claro P.J.A. *J. Mol. Struct*., **469** (1 – 3), 191 (1999).
34. Ribeiro-Claro P.J.A., Amado A.M. *J. Mol. Struct*., **528** (1 – 3), 19 (2000).
35. Anoikin E.V., Mashinsky V.M., Neustruev V.B., Sidorin Y.S. *J. Non-Crystal. Sol*., **179**, 243 (1994).